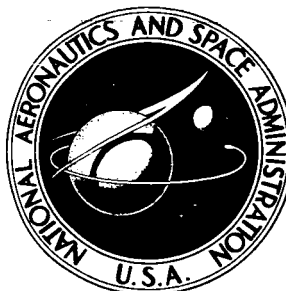**NASA TECHNICAL NOTE**

NASA TN D-4075

NASA TN D-4075

FACILITY FORM 602

N67-32394 (ACCESSION NUMBER) (THRU)

(PAGES) (CODE)
02

(NASA CR OR TMX OR AD NUMBER) (CATEGORY)

THEORETICAL DYNAMIC ANALYSIS OF THE LANDING LOADS ON A VEHICLE WITH A TRICYCLE LANDING GEAR

by Richard B. Noll and James M. McKay

Flight Research Center
Edwards, Calif.

GPO PRICE $ _____

CFSTI PRICE(S) $ _____

Hard copy (HC) _3.00_

Microfiche (MF) _.65_

ff 653 July 65

NATIONAL AERONAUTICS AND SPACE ADMINISTRATION • WASHINGTON, D. C. • AUGUST 1967

THEORETICAL DYNAMIC ANALYSIS OF THE LANDING LOADS

ON A VEHICLE WITH A TRICYCLE LANDING GEAR

By Richard B. Noll and James M. McKay

Flight Research Center
Edwards, Calif.

NATIONAL AERONAUTICS AND SPACE ADMINISTRATION

THEORETICAL DYNAMIC ANALYSIS OF THE LANDING LOADS

ON A VEHICLE WITH A TRICYCLE LANDING GEAR

By Richard B. Noll and James M. McKay
Flight Research Center

SUMMARY

A theoretical analysis is presented for the landing dynamics of a vehicle equipped with a tricycle landing-gear system. The equations are simplified in order to provide a more convenient yet adequate analysis for most vehicles. The adequacy of the simplified analysis for simulating the landing dynamics and loads of a vehicle is illustrated by comparing results of calculations with flight-test data from the X-15 research airplane. The feasibility of using the modified analysis for investigating off-design landing contingencies is demonstrated by examples of studies performed for the X-15.

INTRODUCTION

The dynamics of a conventional tricycle landing-gear system are generally well understood. However, unusual dynamic problems may arise if the basic gear system is modified for use on special types of vehicles where considerations such as simplicity, ease of stowage, resistance to thermal loads, or directional stability on the ground are major design factors. The X-15 research airplane is a prime example of a vehicle with unique landing dynamic problems caused by a modified tricycle gear system (refs. 1 to 4). Although a dynamic analysis had been used in the design of the X-15 gear, it was apparent from flight-test results that the landing dynamics of the complete vehicle system had not been satisfactorily simulated (ref. 4). In order to study the landing dynamics and parameters affecting the landing loads of unusual configurations, the six rigid-body degrees of freedom plus a degree of freedom for each gear were programed for analysis on an analog computer.

A simplified form of the analysis, which is described briefly in reference 2, has proved to be successful in uncovering problems of the X-15 landing dynamics (refs. 2 and 3), in predicting landing loads and simulating actual landings (refs. 2 and 3), and in determining the effects of design changes on landing loads (ref. 4). This paper presents the extensive analysis as well as the simplified X-15 landing-dynamics equations in detail and assesses the validity of the simplifications by comparing them with flight-test results. Analytical predictions of the effects of wing flaps, horizontal-tail loads, and weight on the X-15 landing loads are discussed briefly.

SYMBOLS

Measurements used in this investigation were taken in the U. S. Customary System of Units. Equivalent values are indicated parenthetically in the International System of Units (SI). Details concerning the use of SI, together with physical constants and conversion factors, are given in reference 5.

a_n normal acceleration, g

b wing span, feet (meters)

C_D drag coefficient, $\dfrac{\text{Drag}}{\bar{q}S}$

C_{D_0} drag coefficient at zero angle of attack

C_{D_α} rate of change of drag coefficient with angle of attack, $\dfrac{\partial C_D}{\partial \alpha}$, per degree (radian)

$C_{D_{\delta_h}}$ rate of change of drag coefficient with respect to horizontal-tail deflection, $\dfrac{\partial C_D}{\partial \delta_h}$, per degree (radian)

C_L lift coefficient, $\dfrac{\text{Lift}}{\bar{q}S}$

C_{L_q} rate of change of lift coefficient with pitching angular-velocity factor, $\dfrac{\partial C_L}{\partial \dfrac{q\bar{c}}{2V}}$, per degree (radian)

C_{L_0} lift coefficient at zero angle of attack

C_{L_α} rate of change of lift coefficient with angle of attack, $\dfrac{\partial C_L}{\partial \alpha}$, per degree (radian)

$C_{L_{\dot{\alpha}}}$ rate of change of lift coefficient with rate of change of angle-of-attack factor, $\dfrac{\partial C_L}{\partial \dfrac{\dot{\alpha}\bar{c}}{2V}}$, per degree (radian)

$C_{L_{\delta_h}}$ rate of change of lift coefficient with respect to horizontal-tail deflection, $\dfrac{\partial C_L}{\partial \delta_h}$, per degree (radian)

2

C_l — rolling-moment coefficient, $\dfrac{\text{Rolling moment}}{\bar{q}Sb}$

C_{l_p} — damping-in-roll derivative, $\dfrac{\partial C_l}{\partial \frac{pb}{2V}}$, per degree (radian)

C_{l_r} — rate of change of rolling-moment coefficient with yawing angular-velocity factor, $\dfrac{\partial C_l}{\partial \frac{rb}{2V}}$, per degree (radian)

C_{l_β} — effective dihedral derivative, $\dfrac{\partial C_l}{\partial \beta}$, per degree (radian)

$C_{l_{\dot\beta}}$ — rate of change of rolling-moment coefficient with rate of change of angle-of-sideslip factor, $\dfrac{\partial C_l}{\partial \frac{\dot\beta b}{2V}}$, per degree (radian)

$C_{l_{\delta_a}}$ — rate of change of rolling-moment coefficient with respect to aileron deflection, $\dfrac{\partial C_l}{\partial \delta_a}$, per degree (radian)

$C_{l_{\delta_v}}$ — rate of change of rolling-moment coefficient with respect to vertical-tail deflection, $\dfrac{\partial C_l}{\partial \delta_v}$, per degree (radian)

C_m — pitching-moment coefficient, $\dfrac{\text{Pitching moment}}{\bar{q}S\bar{c}}$

C_{m_q} — rate of change of pitching-moment coefficient with pitching angular-velocity factor, $\dfrac{\partial C_m}{\partial \frac{q\bar{c}}{2V}}$, per degree (radian)

C_{m_0} — pitching-moment coefficient at zero angle of attack

C_{m_α} — longitudinal-stability derivative, $\dfrac{\partial C_m}{\partial \alpha}$, per degree (radian)

$C_{m_{\dot\alpha}}$ — rate of change of pitching-moment coefficient with rate of change of angle-of-attack factor, $\dfrac{\partial C_m}{\partial \frac{\dot\alpha\bar{c}}{2V}}$, per degree (radian)

C_{m_β} — rate of change of pitching-moment coefficient with angle of sideslip, $\dfrac{\partial C_m}{\partial \beta}$, per degree (radian)

3

$C_{m_{\delta_h}}$ — rate of change of pitching-moment coefficient with respect to horizontal-tail deflection, $\dfrac{\partial C_m}{\partial \delta_h}$, per degree (radian)

C_n — yawing-moment coefficient, $\dfrac{\text{Yawing moment}}{\bar{q}Sb}$

C_{n_p} — rate of change of yawing-moment coefficient with rolling angular-velocity factor, $\dfrac{\partial C_n}{\partial \frac{pb}{2V}}$, per degree (radian)

C_{n_r} — damping-in-yaw derivative, $\dfrac{\partial C_n}{\partial \frac{rb}{2V}}$, per degree (radian)

C_{n_β} — directional-stability derivative, $\dfrac{\partial C_n}{\partial \beta}$, per degree (radian)

$C_{n_{\dot\beta}}$ — rate of change of yawing-moment coefficient with rate of change of angle-of-sideslip factor, $\dfrac{\partial C_n}{\partial \frac{\dot\beta b}{2V}}$, per degree (radian)

$C_{n_{\delta_a}}$ — rate of change of yawing-moment coefficient with respect to aileron deflection, $\dfrac{\partial C_n}{\partial \delta_a}$, per degree (radian)

$C_{n_{\delta_v}}$ — rate of change of yawing-moment coefficient with respect to vertical-tail deflection, $\dfrac{\partial C_n}{\partial \delta_v}$, per degree (radian)

C_Y — side-force coefficient, $\dfrac{\text{Side force}}{\bar{q}S}$

C_{Y_p} — rate of change of side-force coefficient with rolling angular-velocity factor, $\dfrac{\partial C_Y}{\partial \frac{pb}{2V}}$, per degree (radian)

C_{Y_r} — rate of change of side-force coefficient with yawing angular-velocity factor, $\dfrac{\partial C_Y}{\partial \frac{rb}{2V}}$, per degree (radian)

C_{Y_β} — side-force derivative, $\dfrac{\partial C_Y}{\partial \beta}$, per degree (radian)

4

$C_{Y_{\dot{\beta}}}$ rate of change of side-force coefficient with rate of change of angle-of-sideslip factor, $\dfrac{\partial C_Y}{\partial \dfrac{\dot{\beta}b}{2V}}$, per degree (radian)

$C_{Y_{\delta_a}}$ rate of change of side-force coefficient with respect to aileron deflection, $\dfrac{\partial C_Y}{\partial \delta_a}$, per degree (radian)

$C_{Y_{\delta_v}}$ rate of change of side-force coefficient with respect to vertical-tail deflection, $\dfrac{\partial C_Y}{\partial \delta_v}$, per degree (radian)

$\bar{c}$ mean aerodynamic chord, feet (meters)

d distance between center of gravity and ground reaction point of gear, measured in y-z plane parallel to z-axis, feet (meters)

$\bar{d}$ distance between center of gravity and gear point of attachment, measured in y-z plane parallel to z-axis, feet (meters)

F_A landing-gear airspring (pneumatic) force, measured normal to the ground plane, pounds (newtons)

F_f landing-gear friction force, measured normal to the ground plane, pounds (newtons)

F_H landing-gear hydraulic force, measured normal to the ground plane, pounds (newtons)

F_h friction force on the landing gear, measured in the ground plane, pounds (newtons)

F_s main-gear shock-strut force, pounds (newtons)

F_v landing-gear reaction normal to the ground plane, pounds (newtons)

F_x, F_y, F_z force measured parallel to x-, y-, and z-axes, respectively, pounds (newtons)

F_δ landing-gear bending or deflection load, measured normal to ground plane, pounds (newtons)

g acceleration due to gravity, feet/second^2 (meters/second^2)

h change in vertical height of point of attachment of gear due to rigid-body rotation about the point of gear contact, feet (meters)

I_x, I_y, I_z	moments of inertia referred to the x-, y-, and z-axes, respectively, slug-foot^2 (kilogram-meter^2)
I_{xz}	product of inertia referred to the x- and z-axes, slug-foot^2 (kilogram-meter^2)
l	distance between center of gravity and ground-contact point of gear, measured in x-z plane parallel to the x-axis, feet (meters)
l_H	distance between center of gravity and gear point of attachment measured in x-z plane parallel to the x-axis, feet (meters)
M_x, M_y, M_z	moments about the x-, y-, and z-axes, respectively, foot-pound (meter-newton)
m	vehicle mass, slugs (kilograms)
p, q, r	rolling, pitching, and yawing angular velocities, respectively, measured about the x-, y-, and z-axes, degrees/second (radians/second)
$\bar{q}$	dynamic pressure, $\frac{1}{2}\rho V^2$, pounds/foot^2 (newtons/meter^2)
R	distance between center of gravity and gear point of attachment, measured in the y-z plane parallel to the y-axis, feet (meters)
R_A	distance between center of gravity and ground-contact point of gear, measured in y-z plane parallel to the y-axis, feet (meters)
S	wing area, foot^2 (meter^2)
u, v, w	translational components of relative velocity vector parallel to x-, y-, and z-axes, respectively, feet/second (meters/second)
u', v', w'	components of center-of-gravity translational velocity parallel to the x-, y-, and z-axes, respectively, feet/second (meters/second)
V	magnitude of vehicle relative velocity, feet/second (meters/second)
V_G	magnitude of relative-velocity vector measured in the ground plane, feet/second (meters/second)
V_v	sink speed (vertical velocity), feet/second (meters/second)
V_w	magnitude of wind velocity, feet/second (meters/second)
V_x', V_y', V_z'	components of center-of-gravity velocity, relative to x-, y-, and z-axes, respectively, feet/second (meters/second)
V_{x_o}', V_{y_o}'	components of center-of-gravity velocity parallel to the x_o- and y_o-axes, respectively, feet/second (meters/second)

6

W	vehicle weight, pounds (newtons)
X, Y, Z	inertial cartesian coordinate system
x, y, z	cartesian coordinates of body-axis system
x_0, y_0, z_0	cartesian coordinates obtained by rotating X-, Y-, and Z-system through Euler angle ψ; distances measured parallel to these axes, feet (meters)
α	angle of attack, degrees (radians)
β	angle of sideslip, degrees (radians)
γ	flight-path angle, degrees (radians)
δ	landing-gear vertical deflection, feet (meters)
δ_a	aileron deflection, degrees (radians)
δ_h	horizontal-tail (elevator) deflection, degrees (radians)
δ_s	main-gear shock-strut deflection, feet (meters)
δ_v	vertical-tail (rudder) deflection, degrees (radians)
λ	angle between the x_0-axis and the friction force on the gear, degrees (radians)
μ	coefficient of friction
ρ	density of air, slugs/cubic foot (kilograms/cubic meter)
ψ, θ, φ	Euler yaw, pitch, and roll angle, respectively, degrees (radians)
ψ_w	angle between wind-velocity vector and X-axis, degrees (radians)

Subscripts:

D	design value
i	body position or gear being considered
max	maximum value
M	both main gear
N	nose gear

o   initial condition at main-gear touchdown

1,2   left and right main gear, respectively

A dot above a quantity denotes the first derivative with respect to time; a double dot denotes the second derivative with respect to time.

ANALYSIS

Equations describing the landing dynamics of a vehicle equipped with a tricycle landing-gear system and unpowered during landing are presented in this section. Vehicle geometry, body-axis coordinate system, landing-gear force vectors, and velocity-vector orientation are shown in figures 1(a) to 1(c) in which the x-, y-, and z-axes are the vehicle body axes and the x-z plane is the vehicle symmetry plane.
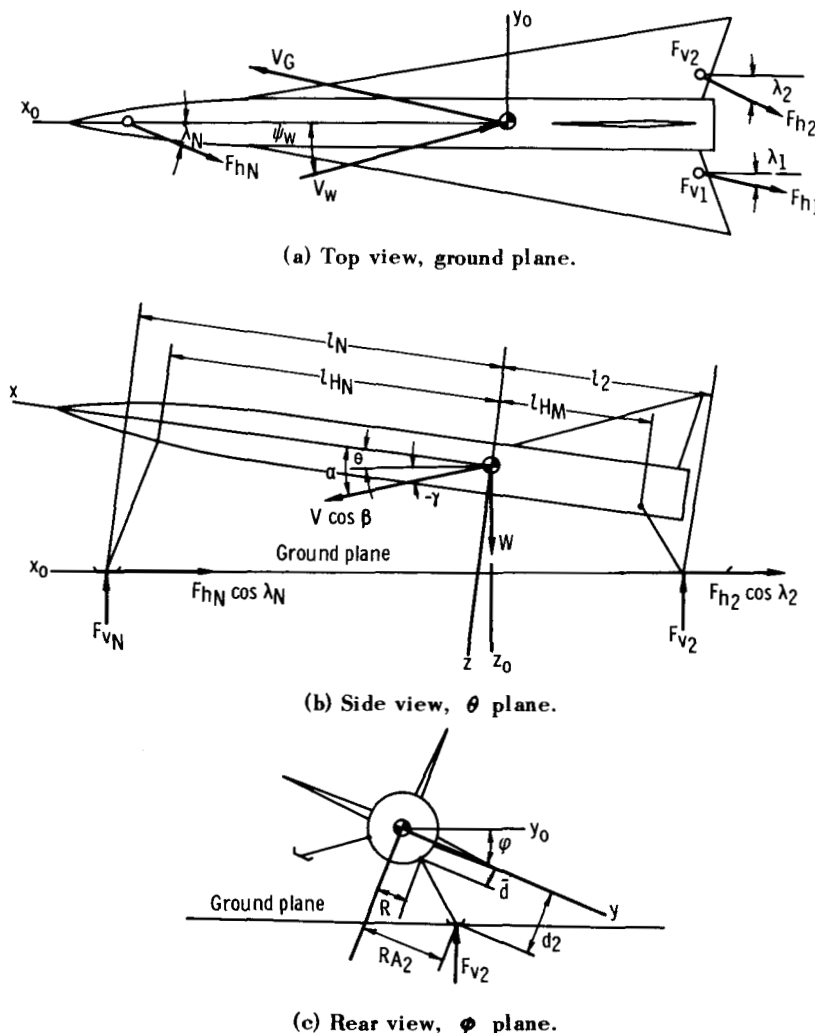

(a) Top view, ground plane.

(b) Side view, θ plane.

(c) Rear view, φ plane.

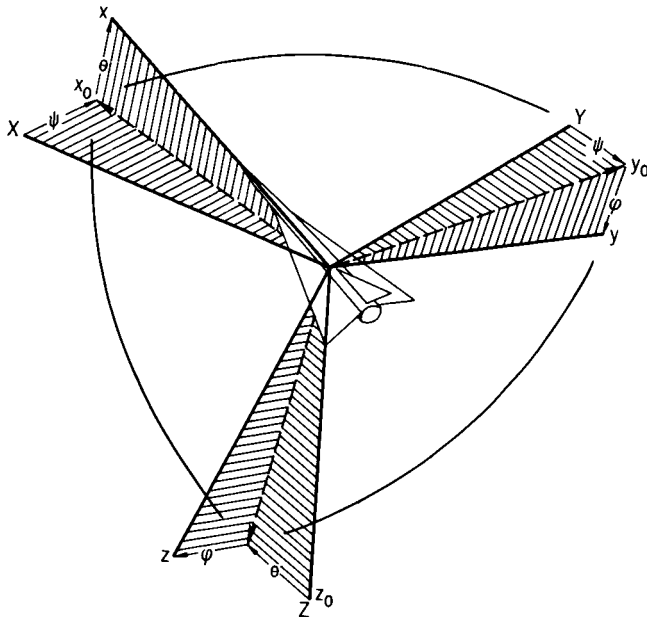Figure 1.— Vehicle geometry and gear loadings.

8

Figure 2.— Orientation of body axes with respect to inertial axes.

The transformation from an inertial coordinate system, X, Y, and Z, to the body axis system, as illustrated in figure 2, is achieved through the Euler angles in the order ψ, θ, and φ. The inertial axes are assumed to lie in the ground plane with the positive X-axis in the direction of the vehicle motion at touchdown. It is convenient to present the instantaneous heading after touchdown in terms of the x_o-, y_o-, and z_o-axis system, which is the inertial system rotated through the Euler, or yaw, angle ψ.

The translation and rotation degree-of-freedom equations of the vehicle center of gravity in body-axis coordinates are written (ref. 6)

$$\sum F_x = -m(\dot{u} + qw - rv) - \bar{q}S\left\{\left(C_{D_0} + C_{D_\alpha}\alpha + C_{D_{\delta_h}}\delta_h\right)\cos\alpha - \left[C_{L_0} + C_{L_\alpha}\alpha + C_{L_{\delta_h}}\delta_h + \frac{\bar{c}}{2V}\left(C_{L_{\dot\alpha}}\dot\alpha + C_{L_q}q\right)\right]\sin\alpha\right\}$$

$$+\left(F_{v_1} + F_{v_2} + F_{v_N}\right)\sin\theta - \left(F_{h_1}\cos\lambda_1 + F_{h_2}\cos\lambda_2 + F_{h_N}\cos\lambda_N\right)\cos\theta - W\sin\theta = 0 \qquad (1a)$$

$$\sum F_y = -m(\dot{v} + ru - pw) + \bar{q}S\left[C_{Y_{\delta_a}}\delta_a + C_{Y_{\delta_v}}\delta_v + C_{Y_\beta}\beta + \frac{b}{2V}\left(C_{Y_r}r + C_{Y_p}p + C_{Y_{\dot\beta}}\dot\beta\right)\right]$$

$$-\left(F_{v_1} + F_{v_2} + F_{v_N}\right)\cos\theta\sin\varphi - F_{h_1}(\cos\varphi\sin\lambda_1 + \sin\theta\sin\varphi\cos\lambda_1)$$

$$-F_{h_2}(\cos\varphi\sin\lambda_2 + \sin\theta\sin\varphi\cos\lambda_2) - F_{h_N}(\cos\varphi\sin\lambda_N + \sin\theta\sin\varphi\cos\lambda_N) + W\cos\theta\sin\varphi = 0 \quad (1b)$$

$$\sum F_z = -m(\dot{w} + pv - qu) - \bar{q}S\left\{\left(C_{D_0} + C_{D_\alpha}\alpha + C_{D_{\delta_h}}\delta_h\right)\sin\alpha + \left[C_{L_0} + C_{L_\alpha}\alpha + C_{L_{\delta_h}}\delta_h + \frac{\bar{c}}{2V}\left(C_{L_{\dot\alpha}}\dot\alpha + C_{L_q}q\right)\right]\cos\alpha\right\}$$

$$-\left(F_{v_1} + F_{v_2} + F_{v_N}\right)\cos\theta\cos\varphi - F_{h_1}(\sin\theta\cos\varphi\cos\lambda_1 - \sin\varphi\sin\lambda_1) - F_{h_2}(\sin\theta\cos\varphi\cos\lambda_2 - \sin\varphi\sin\lambda_2)$$

$$-F_{h_N}(\sin\theta\cos\varphi\cos\lambda_N - \sin\varphi\sin\lambda_N) + W\cos\theta\cos\varphi = 0 \qquad (1c)$$

$$\sum M_x = -I_x \dot{p} + I_{xz}(\dot{r} + pq) + (I_y - I_z)qr + \bar{q}Sb\left[C_{l_{\delta_a}}\delta_a + C_{l_{\delta_v}}\delta_v + C_{l_\beta}\beta + \frac{b}{2V}\left(C_{l_p}p + C_{l_r}r + C_{l_{\dot\beta}}\dot\beta\right)\right]$$

$$+ F_{v_1}\left(R_{A_1}\cos\varphi + d_1\sin\varphi\right)\cos\theta - F_{v_2}\left(R_{A_2}\cos\varphi - d_2\sin\varphi\right)\cos\theta + F_{v_N}d_N\cos\theta\sin\varphi$$

$$+ F_{h_1}\left[\left(R_{A_1}\cos\varphi + d_1\sin\varphi\right)\sin\theta\cos\lambda_1 - \left(R_{A_1}\sin\varphi - d_1\cos\varphi\right)\sin\lambda_1\right]$$

$$- F_{h_2}\left[\left(R_{A_2}\cos\varphi - d_2\sin\varphi\right)\sin\theta\cos\lambda_2 - \left(R_{A_2}\sin\varphi + d_2\cos\varphi\right)\sin\lambda_2\right]$$

$$+ F_{h_N}d_N\left(\cos\varphi\sin\lambda_N + \sin\theta\sin\varphi\cos\lambda_N\right) = 0 \tag{1d}$$

$$\sum M_y = -I_y\dot{q} + (I_z - I_x)pr + I_{xz}(r^2 - p^2) + \bar{q}S\bar{c}\left[C_{m_0} + C_{m_\alpha}\alpha + C_{m_{\delta_h}}\delta_h + C_{m_\beta}\beta + \frac{\bar{c}}{2V}\left(C_{m_{\dot\alpha}}\dot\alpha + C_{m_q}q\right)\right]$$

$$+ F_{v_1}(d_1\sin\theta - l_1\cos\theta\cos\varphi) + F_{v_2}(d_2\sin\theta - l_2\cos\theta\cos\varphi) + F_{v_N}(d_N\sin\theta + l_N\cos\theta\cos\varphi)$$

$$+ F_{h_1}\left[l_1\sin\varphi\sin\lambda_1 - (l_1\sin\theta\cos\varphi + d_1\cos\theta)\cos\lambda_1\right]$$

$$+ F_{h_2}\left[l_2\sin\varphi\sin\lambda_2 - (l_2\sin\theta\cos\varphi + d_2\cos\theta)\cos\lambda_2\right]$$

$$- F_{h_N}\left[l_N\sin\varphi\sin\lambda_N - (l_N\sin\theta\cos\varphi - d_N\cos\theta)\cos\lambda_N\right] = 0 \tag{1e}$$

$$\sum M_z = -I_z\dot{r} + I_{xz}(\dot{p} - qr) + (I_x - I_y)pq + \bar{q}Sb\left[C_{n_{\delta_a}}\delta_a + C_{n_{\delta_v}}\delta_v + C_{n_\beta}\beta + \frac{b}{2V}\left(C_{n_r}r + C_{n_p}p + C_{n_{\dot\beta}}\dot\beta\right)\right]$$

$$+ F_{v_1}\left(R_{A_1}\sin\theta + l_1\cos\theta\sin\varphi\right) - F_{v_2}\left(R_{A_2}\sin\theta - l_2\cos\theta\sin\varphi\right) - F_{v_N}l_N\cos\theta\sin\varphi$$

$$+ F_{h_1}\left[l_1\cos\varphi\sin\lambda_1 + (l_1\sin\theta\sin\varphi - R_{A_1}\cos\theta)\cos\lambda_1\right]$$

$$+ F_{h_2}\left[l_2\cos\varphi\sin\lambda_2 + (l_2\sin\theta\sin\varphi + R_{A_2}\cos\theta)\cos\lambda_2\right]$$

$$- F_{h_N}l_N(\cos\varphi\sin\lambda_N + \sin\theta\sin\varphi\cos\lambda_N) = 0 \tag{1f}$$

where landing-gear contributions to the forces and moments are recognized as the terms involving the vertical forces on the gear F_v and the drag forces on the gear F_h.

The aerodynamic coefficients included in equations (1) are those most commonly used for aircraft stability and control analyses; however, the importance of each derivative and the possible inclusion of others will depend on the vehicle configuration being considered.

Landing-Gear Analysis

The deflection of the landing gear, such as gear bending and tire deflection, constitutes additional degrees of freedom. The importance of these deflections on the

10

loads is dependent on the type of gear being considered. In addition to the deflections, it is necessary to consider equipment provided for energy absorption. Again, the type of gear limits generalization of the analysis; however, since most aircraft landing gear utilize oleopneumatic shock struts, this type of strut will be discussed.

Oleopneumatic shock struts do not begin to deflect during impact until sufficient force is developed to overcome the preload or breakout force caused by the inflation pressure and by friction. Before this instant, the shock strut is effectively rigid in compression and the gear load is a function of the gear structural or tire deflection, or both, or

$$F_{V_i} = F_{\delta_i} \tag{2}$$

As the vehicle descent continues, the preload is exceeded and the shock strut begins to displace. The gear vertical reactions become

$$F_{V_i} = F_{A_i} + F_{H_i} + F_{f_i} \tag{3}$$

where the airspring load F_A is a function of the shock-strut displacement, and the hydraulic load F_H is a function of both the displacement and the rate of displacement of the shock strut. The friction load F_f is determined by the normal load on the shock-strut-cylinder bearing surfaces and the coefficients of friction of the surfaces.

The overall rate of vertical deflection of the gear is related to the center-of-gravity vertical velocity by (ref. 6)

$$\dot{\delta}_i = \dot{h}_i + \dot{z}_o - \left[l_{H_i} \cos\theta + (\bar{d}_i \cos\varphi + R_i \sin\varphi) \sin\theta \right] \dot{\theta} + (R_i \cos\varphi - \bar{d}_i \sin\varphi) \dot{\varphi} \cos\theta \tag{4}$$

where the dimension l_{H_i} is positive for nose gear and negative for main gear; R_i is positive for right main gear, negative for left main gear, and zero for nose gear; $\bar{d}_i$ is positive for all gear; and $\dot{h}_i$ is the rate of change of vertical height of point of attachment due to rigid-body rotation about the point of gear contact. The equations are arranged so that a positive rate indicates shock-strut compression.

The analysis of the gear loads and associated gear and shock-strut deflections depends upon the structure and geometry of the gear as well as the characteristics of the shock struts. An example of a detailed analysis of a gear system equipped with oleopneumatic shock struts is given in appendix A.

Auxiliary Equations

Additional information pertinent to the landing-dynamics equations is given in the following relationships.

The body and Euler rotational rates are related as

$$\left. \begin{aligned} p &= \dot{\varphi} - \dot{\psi} \sin \theta \\ q &= \dot{\theta} \cos \varphi + \dot{\psi} \cos \theta \sin \varphi \\ r &= \dot{\psi} \cos \theta \cos \varphi - \dot{\theta} \sin \varphi \end{aligned} \right\} \tag{5}$$

The definitions of sideslip angle and angle of attack

$$\left. \begin{aligned} \beta &= \sin^{-1} \frac{v}{V} \\ \alpha &= \tan^{-1} \frac{w}{u} \end{aligned} \right\} \tag{6}$$

yield the following relative-velocity components:

$$\left. \begin{aligned} v &= V \sin \beta \\ u &= V \cos \beta \cos \alpha \\ w &= V \cos \beta \sin \alpha \end{aligned} \right\} \tag{7}$$

The vertical velocity $\dot{z}_O$ of the center of gravity, which is related to the rate of vertical deflection of the gear by equation (4), is also related to the relative-velocity components of equations (7) by

$$\dot{z}_O = -u \sin \theta + v \sin \varphi \cos \theta + w \cos \varphi \cos \theta \tag{8}$$

Substitution of equations (7) into equation (8) results in the following angular relationship:

$$\sin \gamma = \cos \beta \cos \alpha \sin \theta - (\sin \beta \sin \varphi + \cos \beta \sin \alpha \cos \varphi) \cos \theta \tag{9}$$

12

where the flight-path angle γ is defined by

$$\gamma = \sin^{-1} \frac{-\dot{z}_o}{V} \tag{10}$$

The gear horizontal load at the ground-contact point is proportional to the gear reaction normal to the ground and is expressed as

$$F_{h_i} = \mu_i F_{v_i} \tag{11}$$

The trigonometric relations for the friction force angles λ_i are given in reference 6 as follows:

$$\left.\begin{aligned}
\cos \lambda_i &= \frac{\left(V'_{x_o}\right)_i}{\left(V_G\right)_i} \\[2em]
\sin \lambda_i &= \frac{\left(V'_{y_o}\right)_i}{\left(V_G\right)_i}
\end{aligned}\right\} \tag{12}$$

where

$$\left.\begin{aligned}
\left(V_G\right)_i^2 &= \left(V'_{x_o}\right)_i^2 + \left(V'_{y_o}\right)_i^2 \\[1.5em]
\left(V'_{x_o}\right)_i &= V'_{x_i} \cos \theta + \left(V'_{y_i} \sin \varphi + V'_{z_i} \cos \varphi\right) \sin \theta \\[1.5em]
\left(V'_{y_o}\right)_i &= V'_{y_i} \cos \varphi - V'_{z_i} \sin \varphi
\end{aligned}\right\} \tag{13}$$

and

$$\left.\begin{aligned}
V'_{x_i} &= u' + qz_i - ry_i \\[1.5em]
V'_{y_i} &= v' + rx_i - pz_i \\[1.5em]
V'_{z_i} &= w' + py_i - qx_i
\end{aligned}\right\} \tag{14}$$

13

$$u' = \left[V \cos \beta - V_w \left(\cos \psi_w \cos \psi + \sin \psi_w \sin \psi \right) \right] \cos \theta$$

$$v' = V \sin \beta - V_w \left[\left(\sin \psi_w \cos \psi - \cos \psi_w \sin \psi \right) \cos \varphi \right.$$

$$\left. + \left(\cos \psi_w \cos \psi + \sin \psi_w \sin \psi \right) \sin \theta \sin \varphi \right] \tag{15}$$

$$w' = V \cos \beta \sin \theta - V_w \left[\left(\cos \psi_w \cos \psi + \sin \psi_w \sin \psi \right) \sin \theta \cos \varphi \right.$$

$$\left. - \left(\sin \psi_w \cos \psi - \cos \psi_w \sin \psi \right) \sin \varphi \right]$$

Simplified Landing-Dynamics Equations for a Vehicle With Tricycle Landing Gear

The equations presented in the preceding section provide an analysis of the landing dynamics of a rigid flight vehicle which is unpowered during landing. A solution of these equations, while not impossible, becomes very complex and time consuming. However, it is possible to simplify the solution by making several assumptions.

One approximation is that the landing is made symmetrically; that is, both main gear impact simultaneously, the vehicle roll and yaw rates are zero, and the vehicle has no sideslip. In addition, if there is no wind and if lateral control inputs are not made, that is,

$$\left. \begin{array}{c} V_w = 0 \\[2ex] \delta_a = 0 \\[2ex] \delta_v = 0 \end{array} \right\} \tag{16}$$

the symmetry of the landing will be maintained. These restraints on the vehicle motion imply that

$$\left. \begin{array}{ll} \dot{\beta} = 0 & \beta = 0 \\[2ex] \dot{\psi} = 0 & \psi = \text{constant} \\[2ex] \dot{\varphi} = 0 & \varphi = 0 \end{array} \right\} \tag{17}$$

14

The symmetry of the vehicle and the assumption of maintaining symmetrical landing conditions result in

$$
\left.
\begin{aligned}
l_1 &= l_2 = l_M \\[12pt]
d_1 &= d_2 = d_M \\[12pt]
R_{A_1} &= R_{A_2} = R_{A_M} \\[12pt]
\dot{\delta}_1 &= \dot{\delta}_2 = \dot{\delta}_M \\[12pt]
F_{v_1} &= F_{v_2} = F_{v_M}
\end{aligned}
\right\}
\tag{18}
$$

Substitution of the auxiliary equations (5), (7), (8), and (11) into the equilibrium equations (1) and (4) yields, upon application of equations (16), (17), and (18), the following landing-dynamics equations for a vehicle with a tricycle landing gear:

$$
\sum F_x = -m\left(\dot{V}\cos\alpha + V\dot{\gamma}\sin\alpha\right) - \bar{q}S\left\{\left(C_{D_0} + C_{D_\alpha}\alpha + C_{D_{\delta_h}}\delta_h\right)\cos\alpha - \left[C_{L_0} + C_{L_\alpha}\alpha + C_{L_{\delta_h}}\delta_h + \frac{\bar{c}}{2V}\left(C_{L_{\dot\alpha}}\dot\alpha + C_{L_q}\dot\theta\right)\right]\sin\alpha\right\}
$$

$$
+ \left(2F_{v_M} + F_{v_N}\right)\sin\theta - \left(2\mu_M F_{v_M} + \mu_N F_{v_N}\right)\cos\theta - W\sin\theta = 0 \tag{19a}
$$

$$
\sum F_y = 0 \tag{19b}
$$

$$
\sum F_z = -m\left(\dot{V}\sin\alpha - V\dot{\gamma}\cos\alpha\right) - \bar{q}S\left\{\left(C_{D_0} + C_{D_\alpha}\alpha + C_{D_{\delta_h}}\delta_h\right)\sin\alpha + \left[C_{L_0} + C_{L_\alpha}\alpha + C_{L_{\delta_h}}\delta_h + \frac{\bar{c}}{2V}\left(C_{L_{\dot\alpha}}\dot\alpha + C_{L_q}\dot\theta\right)\right]\cos\alpha\right\}
$$

$$
- \left(2F_{v_M} + F_{v_N}\right)\cos\theta - \left(2\mu_M F_{v_M} + \mu_N F_{v_N}\right)\sin\theta + W\cos\theta = 0 \tag{19c}
$$

$$
\sum M_x = 0 \tag{19d}
$$

$$
\sum M_y = -I_y\ddot{\theta} + \bar{q}S\bar{c}\left[C_{m_0} + C_{m_\alpha}\alpha + C_{m_{\delta_h}}\delta_h + \frac{\bar{c}}{2V}\left(C_{m_{\dot\alpha}}\dot\alpha + C_{m_q}\dot\theta\right)\right] + 2F_{v_M}\left[d_M(\sin\theta - \mu_M\cos\theta) - l_M(\cos\theta + \mu_M\sin\theta)\right]
$$

$$
+ F_{v_N}\left[d_N(\sin\theta - \mu_N\cos\theta) + l_N(\cos\theta + \mu_N\sin\theta)\right] = 0 \tag{19e}
$$

$$
\sum M_z = 0 \tag{19f}
$$

15

Also

$$\dot{\delta}_M = \dot{h}_M - V \sin \gamma + \left(l_{H_M} \cos \theta - \bar{d}_M \sin \theta\right) \dot{\theta} \left.\vphantom{\begin{array}{c}1\\1\\1\\1\end{array}}\right\}$$

$$\dot{\delta}_N = \dot{h}_N - V \sin \gamma - \left(l_{H_N} \cos \theta + \bar{d}_N \sin \theta\right) \dot{\theta} \left.\vphantom{\begin{array}{c}1\\1\\1\\1\end{array}}\right\} \qquad (20)$$

It should be noted that the restraints expressed in equations (17) reduce auxiliary equation (9) to the familiar form of

$$\alpha = \theta - \gamma \qquad (21)$$

Equations (19) along with equation (21) form a set of four equations for determining V, γ, θ, and α. Equation (3) for the gear loads is valid but remains dependent on the particular gear configuration. The motions of the vehicle and the gear system are related by equations (20).

Simplified Landing-Dynamics Equations for the X-15 Airplane

Landing experience with the X-15 airplane (fig. 3) revealed that once main-gear touchdown occurs, nose-gear impact follows in a short period of time (refs. 1 to 4).
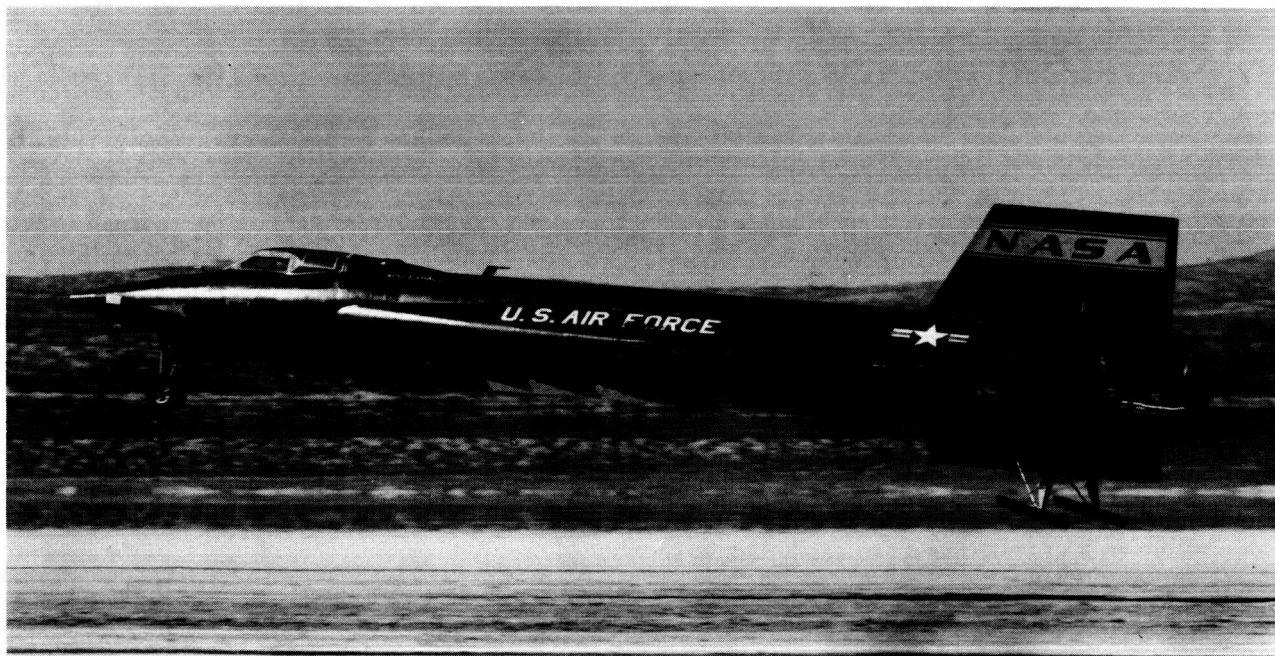

E-7469

Figure 3.— X-15 airplane during landing.

This fact allows two simplifying approximations to be made to the equations of the previous section. First, the velocity of the X-15 can be assumed to be constant during the landing phase, or

$$V = \text{constant} \qquad \dot{V} = 0$$

Second, the pitch attitude θ and angle of attack α reduce to small angles very rapidly so that small-angle approximation may be used as

$$\sin(\theta, \ \alpha) = \theta, \ \alpha$$

$$\cos(\theta, \ \alpha) = 1$$

Application of these approximations to equations (19) results in

$$\sum F_z = mV\dot{\gamma} - \bar{q}S\left[\left(C_{D_0} + C_{D_\alpha}\alpha + C_{D_{\delta_h}}\delta_h\right)\alpha + C_{L_0} + C_{L_\alpha}\alpha + C_{L_{\delta_h}}\delta_h + \frac{\bar{c}}{2V}\left(C_{L_{\dot{\alpha}}}\dot{\alpha} + C_{L_q}\dot{\theta}\right)\right] - 2F_{v_M}\left(1 + \mu_M\theta\right)$$

$$- F_{v_N}\left(1 + \mu_N\theta\right) + W = 0 \tag{22a}$$

$$\sum M_y = -I_y\ddot{\theta} + \bar{q}S\bar{c}\left[C_{m_0} + C_{m_\alpha}\alpha + C_{m_{\delta_h}}\delta_h + \frac{\bar{c}}{2V}\left(C_{m_{\dot{\alpha}}}\dot{\alpha} + C_{m_q}\dot{\theta}\right)\right] + 2F_{v_M}\left[d_M\left(\theta - \mu_M\right) - l_M\left(1 + \mu_M\theta\right)\right]$$

$$+ F_{v_N}\left[d_N\left(\theta - \mu_N\right) + l_N\left(1 + \mu_N\theta\right)\right] = 0 \tag{22b}$$

Equations (22) along with equation (21) form a set of landing-dynamics equations for the parameters θ, γ, and α. Note that the equation for summation of forces in the x-direction, which provides information about drag forces on the airplane, has not been included.

Since the rate of change in vertical height due to rigid-gear rotation $\dot{h}$ is normally small compared to the gear-deflection rates, the overall gear vertical deflections (eqs. (20)) become

$$\left. \begin{aligned} \dot{\delta}_M &= -V\gamma + \left(l_{H_M} - \bar{d}_M\theta\right)\dot{\theta} \\ \dot{\delta}_N &= -V\gamma - \left(l_{H_N} + \bar{d}_N\theta\right)\dot{\theta} \end{aligned} \right\} \tag{23}$$

Also, because of the small-angle approximation

$$\mu_M \theta \ll 1$$

$$\mu_N \theta \ll 1$$

$$C_D \alpha \ll C_L$$

$$\bar{d}_M \theta \ll l_{H_M}$$

$$\bar{d}_N \theta \ll l_{H_N}$$

and the simplified equations for the landing dynamics of the X-15 become

$$mV\dot{\gamma} = \bar{q}S\left[C_{L_0} + C_{L_\alpha}\alpha + C_{L_{\delta_h}}\delta_h + \frac{\bar{c}}{2V}\left(C_{L_{\dot{\alpha}}}\dot{\alpha} + C_{L_q}\dot{\theta}\right)\right] + 2F_{v_M} + F_{v_N} - W \tag{24a}$$

$$I_y\ddot{\theta} = \bar{q}S\bar{c}\left[C_{m_0} + C_{m_\alpha}\alpha + C_{m_{\delta_h}}\delta_h + \frac{\bar{c}}{2V}\left(C_{m_{\dot{\alpha}}}\dot{\alpha} + C_{m_q}\dot{\theta}\right)\right] + 2F_{v_M}\left[d_M\left(\theta - \mu_M\right) - l_M\right] + F_{v_N}\left[d_N\left(\theta - \mu_N\right) + l_N\right] \tag{24b}$$

$$\left.\begin{aligned}\dot{\delta}_M &= -V\gamma + l_{H_M}\dot{\theta} \\ \dot{\delta}_N &= -V\gamma - l_{H_N}\dot{\theta}\end{aligned}\right\} \tag{24c}$$

$$\left.\begin{aligned}F_{v_M} &= F_{A_M} + F_{H_M} + F_{f_M} \\ F_{v_N} &= F_{A_N} + F_{H_N} + F_{f_N}\end{aligned}\right\} \tag{24d}$$

Equations (24) with equation (21) form a complete set of equations for analyzing the landing dynamics of the X-15 airplane. A detailed presentation of the X-15 gear vertical reactions for determining equations (24d) is given in appendix A.

RESULTS AND DISCUSSION

The landing dynamics of a flight vehicle equipped with a tricycle oleopneumatic landing-gear system are presented in equations (1) to (4). This set of equations describes the dynamics of a rigid-body vehicle during landing impact, including

rolling, pitching, and yawing motions, variable aerodynamics and coefficients of friction, and the effects of pilot control inputs. These equations can be simplified to the form of equations (19) and (20) if the landing is made symmetrically. For the specific example of the X-15 airplane, the rapid pitch down at landing (refs. 1 to 4) allows a further simplification of the landing dynamics described by equations (24).

The analysis was verified by comparing results of calculations for equations (24) with experimental results from the X-15 airplane. Initially, computations were made by using the gear-load curves shown in figure 4, which are based on analytical and experimental data, rather than the procedure outlined in appendix A. The total vertical-load curve presents the ratio of vertical load to the design vertical load at the main-gear skid as a function of the ratio of vertical deflection to the maximum vertical deflection of the gear. Velocity-sensitive curves for an arbitrary range of sink speed V_V are shown. The orifice opens at approximately the same deflection for each sink speed,
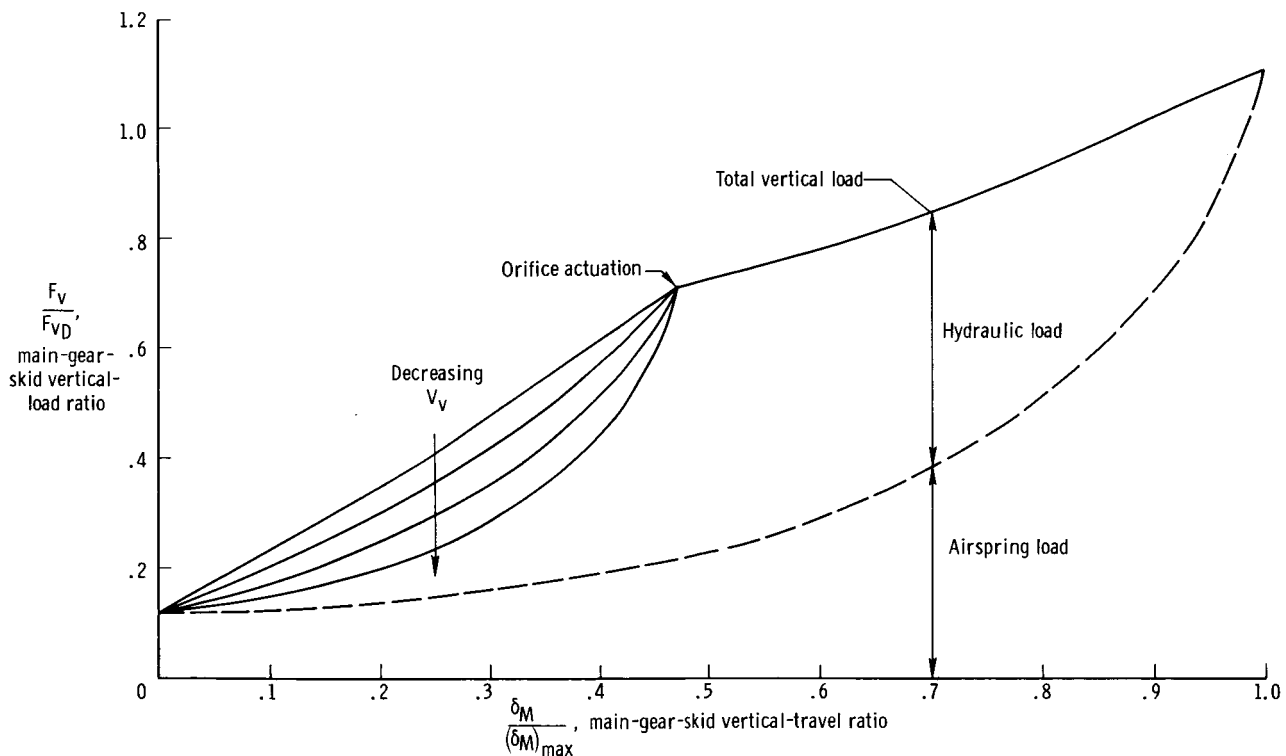

Figure 4.— Approximate variation of X-15 main-gear-skid load with skid vertical travel and sink speed derived from analytical and experimental data.

resulting in the single curve to the maximum deflection; that is, $\dfrac{\delta_M}{\left(\delta_M\right)_{max}} = 1.0$. It should be noted that once orificing occurs the load is independent of sink speed and relatively independent of deflection until large deflections occur. As maximum deflection of the shock strut is approached, the airspring load becomes predominant, since the hydraulic load is negligible as a result of decreased strut velocity.

19

Flight-test results and computations based on the total vertical-load curve of figure 4 were compared in reference 2. The comparison is reproduced in this paper as figure 5. It is apparent that the calculated vertical skid load agrees well with the flight-test results. The simplified analysis predicted the existence of a second reaction as well as the magnitude of the first and second reactions, thereby verifying the dynamic simulation of the landing dynamics.
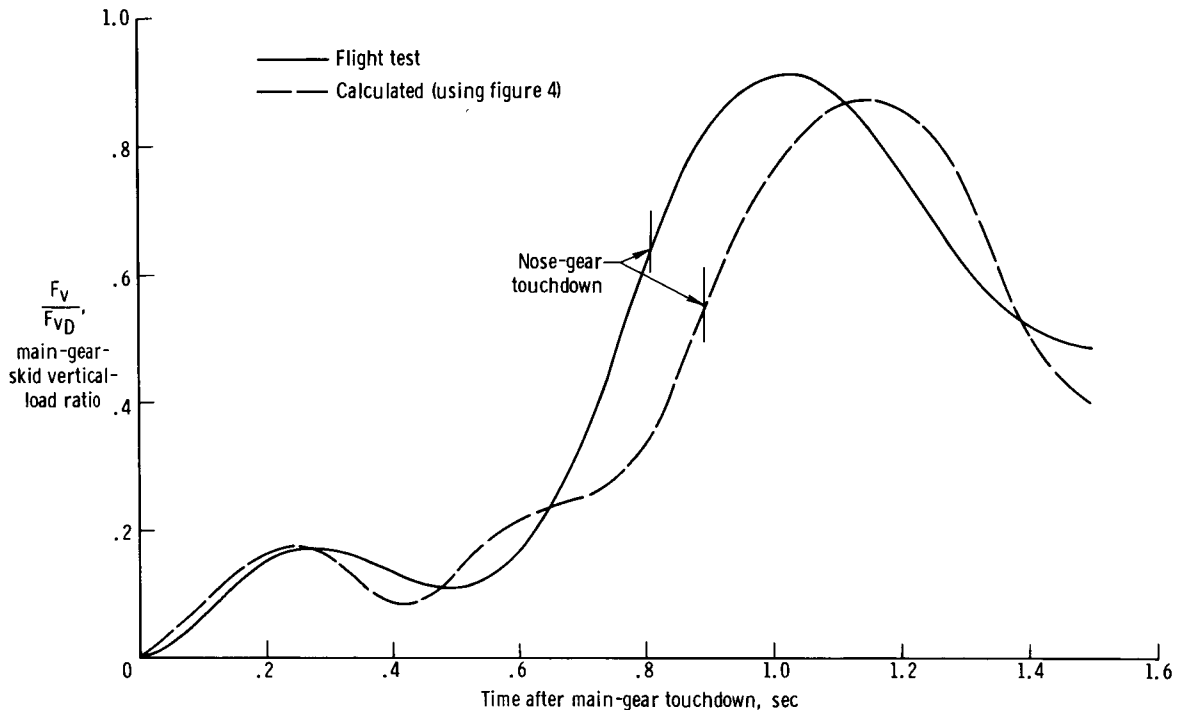

Figure 5.— Comparison of X-15 main-gear-skid-load time histories (from ref. 2).

The simplified analysis based on figure 4 provided extensive information on the effects of various parameters such as gear position and sink speed (refs. 2 and 4). After an emergency landing of the X-15 airplane (ref. 4), the landing analysis was used to simulate the landing and to predict the results of severe off-design landing conditions. It was at this point that the deficiencies of the load curve of figure 4 were realized. Since the gear-load curve was obtained for conditions within the design envelope of the gear, attempts to use the curve for off-design conditions produced unrealistic results. Therefore, the landing-gear-dynamics equations of appendix A were incorporated into the analysis.

In order to provide confidence in the modified analysis, the experimental drop tests of the landing gear were simulated. The basic landing equations were simplified as shown in appendix B. Drop-test and analytical results for the main gear and nose gear are compared in figures 6(a) and 6(b); the agreement is considered to be satisfactory.
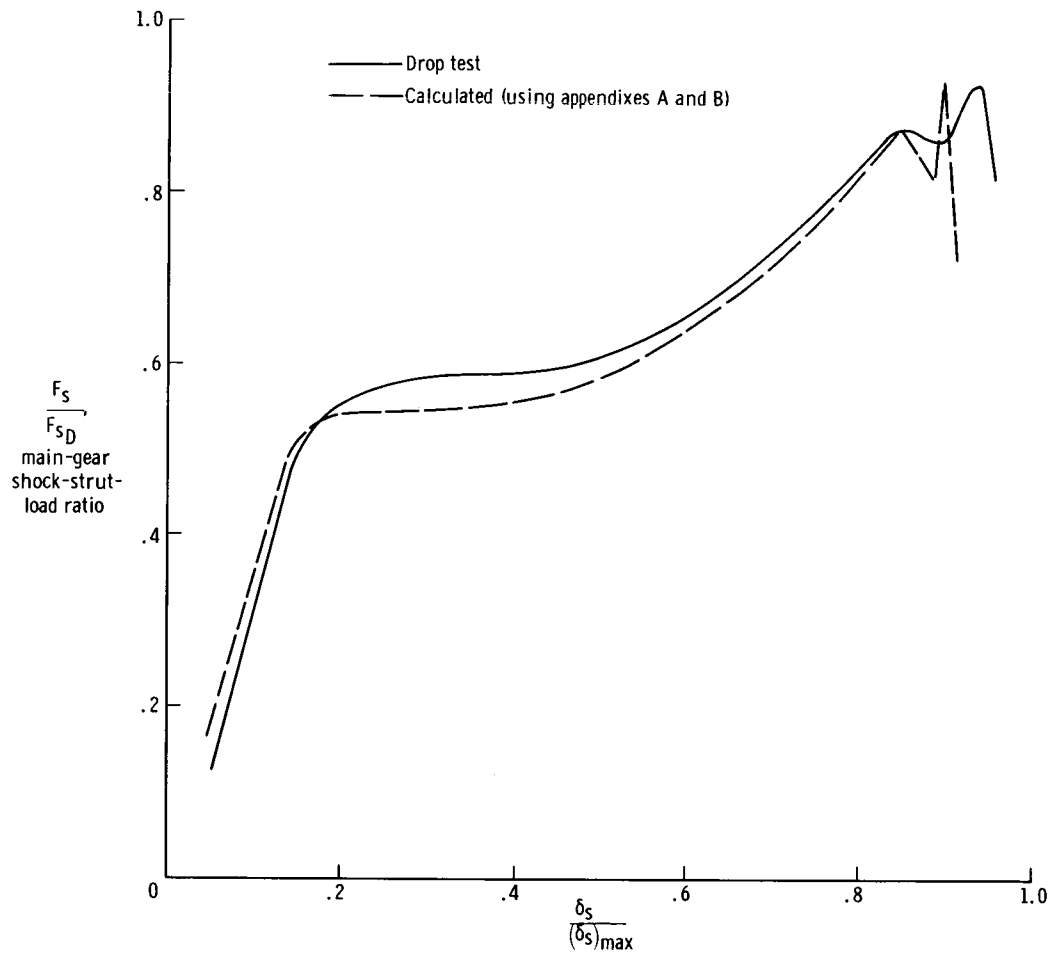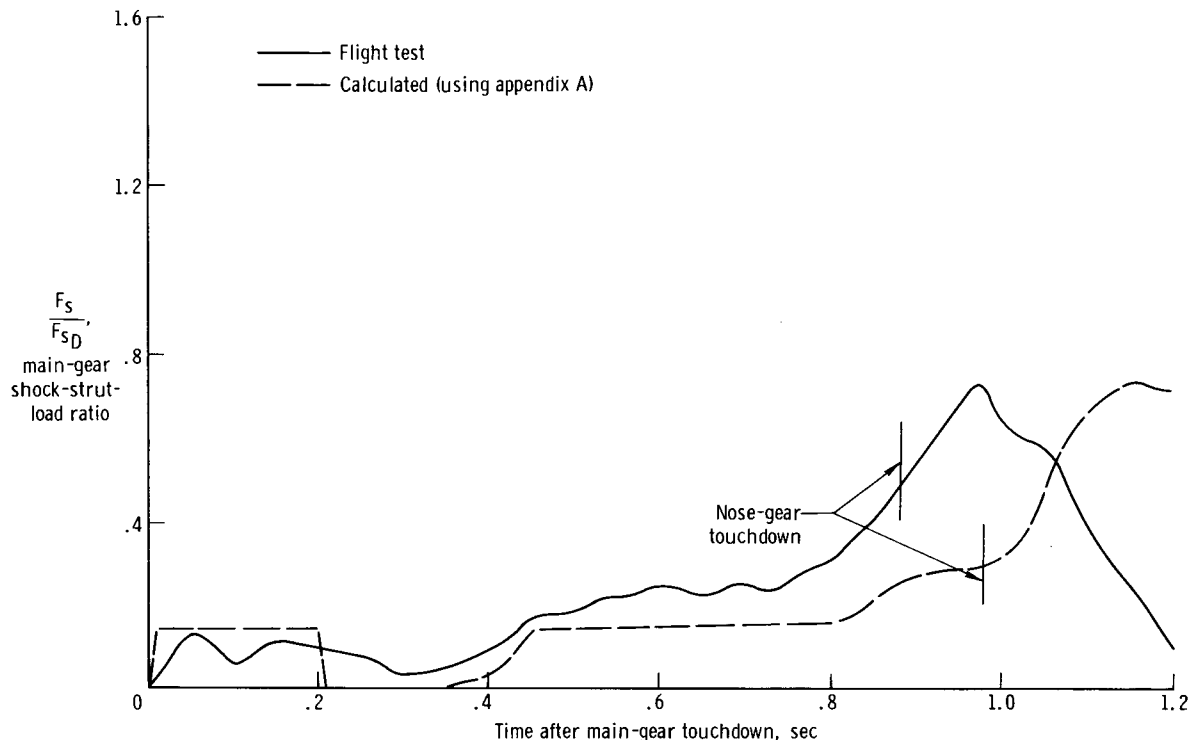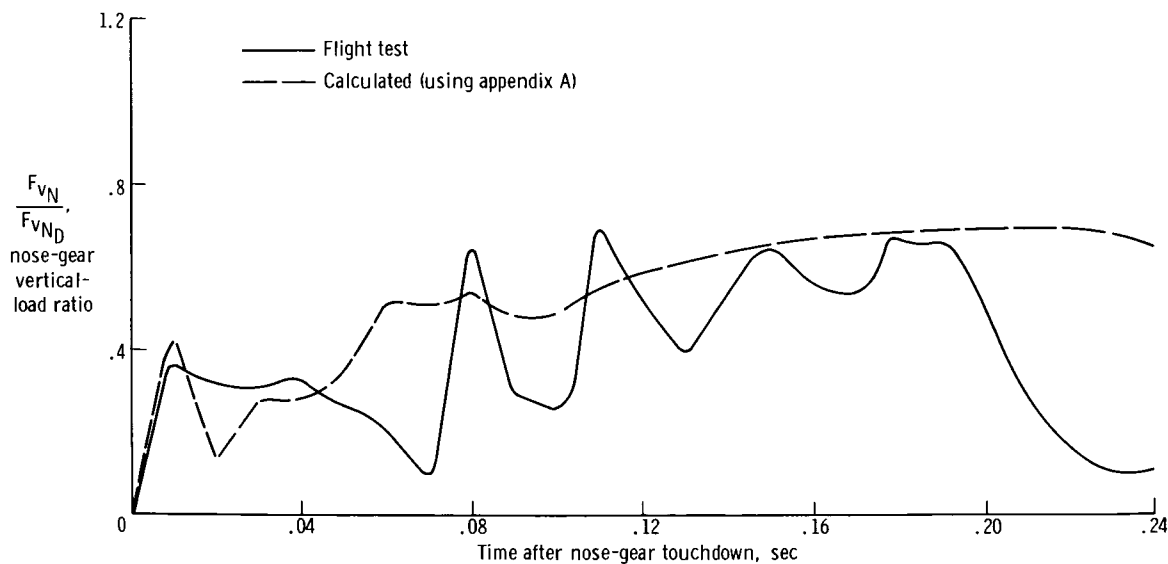
(a) Main gear.
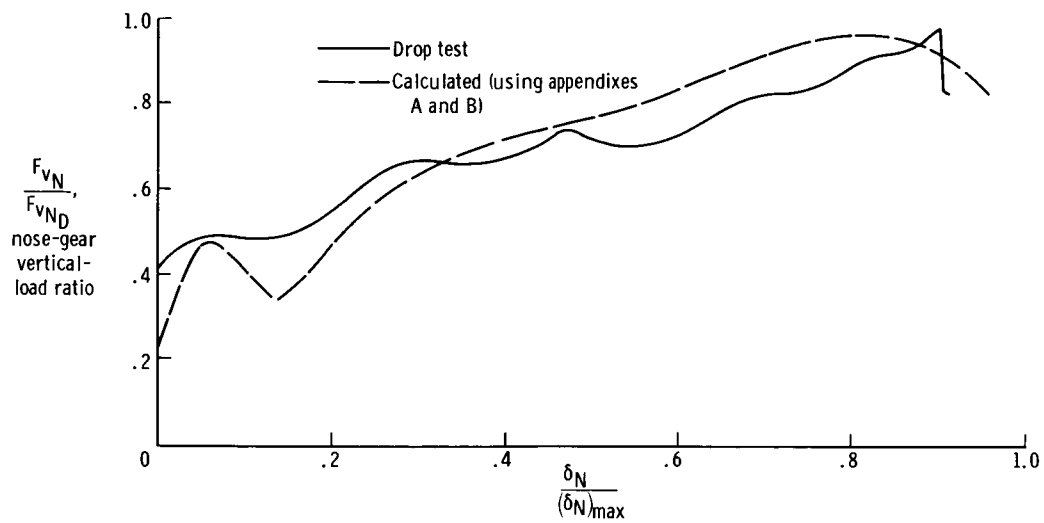
(b) Nose gear.

Figure 6.— Comparison of calculated shock-strut load with drop-test data.

21

The results shown in figure 6 provide confidence in the analysis, but the proper simulation of the landing dynamics of the vehicle system is required as final proof of the validity of the analysis. Results from flight tests and the modified analysis are compared in figure 7. The good agreement obtained in predicting the magnitudes of the first and second reactions as well as a reasonable comparison of overall time

(a) Main gear.

(b) Nose gear.

Figure 7.— Comparison of flight-test and calculated shock-strut time histories.

$$\frac{a_o}{a_D} = 1.06; \quad \frac{V_{v_o}}{V_{v_D}} = 0.20; \quad \frac{W_o}{W_D} = 0.99.$$

22

history for the main gear (fig. 7(a)) indicates that the modified analysis yields accept-
able results. The nose-gear time histories, compared in figure 7(b), reveal that,
although the magnitude of the peak reaction is predicted satisfactorily, the nose-gear
dynamics are not simulated precisely. The discrepancies in the simulation are attrib-
uted to the neglect of nose-gear-tire spin-up loads and strut-bending characteristics.
Similar comments are applicable to most main landing gear. For the X-15 main
gear, however, metal skids are used in place of wheels and tires and no bending
moments are applied to the shock strut, since drag loads are absorbed by drag links
attached at the skids and vertical loads are applied to the shock strut through a bell-
crank (see ref. 1 for description of the X-15 landing-gear system).

The capability of analytically simulating the landing dynamics of a vehicle provides
a valuable tool for assessing operational problems or studying the effects of unusual
configurations as well as for evaluating design concepts. Equally important for
research vehicles, such as the X-15, is the capability of investigating off-design or
emergency landing conditions for which it is unrealistic to obtain flight-test data. The
analysis can be used to determine the severity of the contingencies and to devise pos-
sible emergency procedures for minimizing the landing loads. As an example, main-
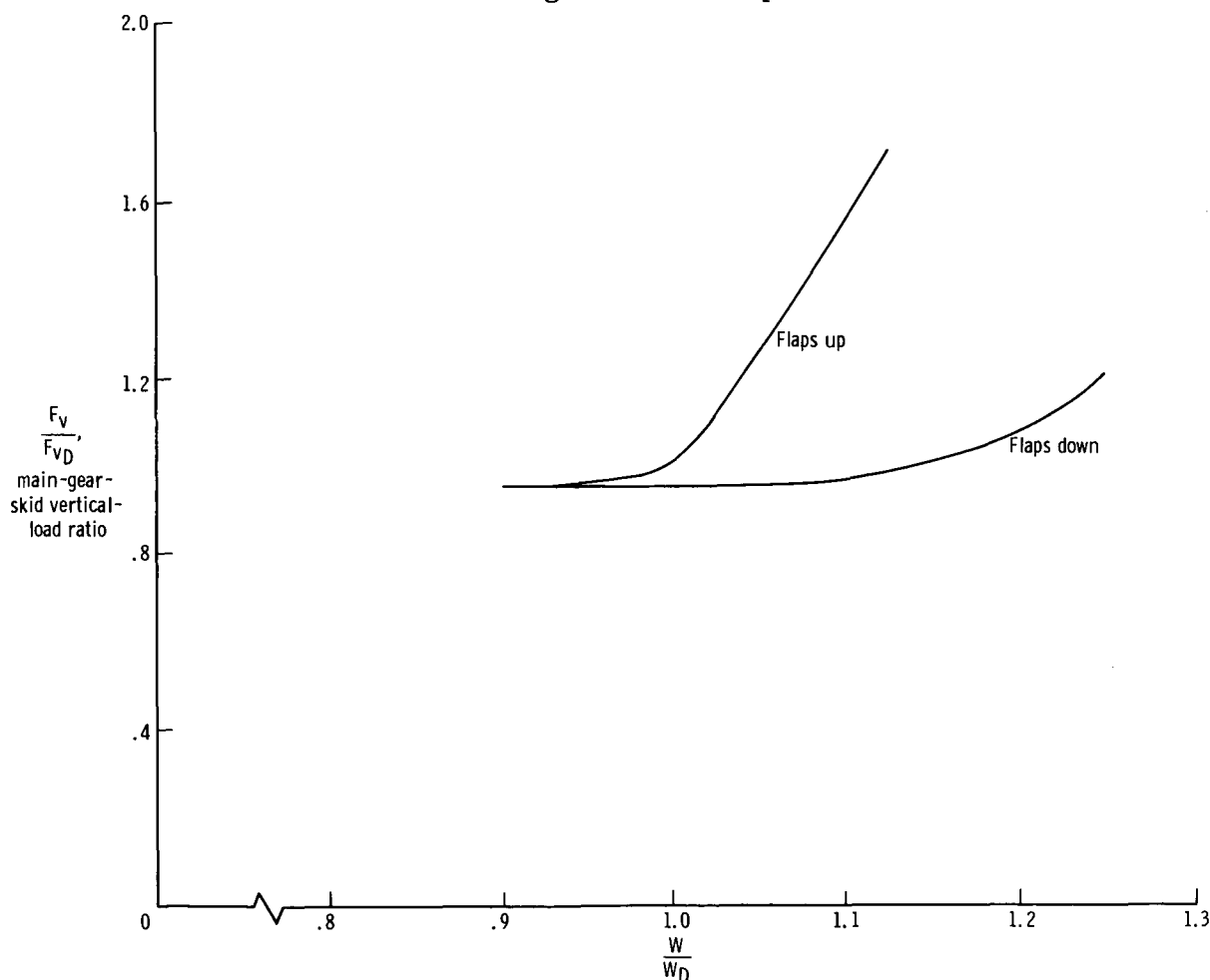gear loads are shown for the X-15 in figure 8 for a flap malfunction and excessive

Figure 8.— Influence of airplane landing weight and flap position on maximum main-gear load calculated by using method of appendix A. $\frac{V_{v_0}}{V_{v_D}} = 0.55$; $\frac{a_0}{a_D} = 1.0$; $\delta_{h_{trim}}$; $a_n = 1g$.

landing weights.   The normal landing condition, in which flaps are used, is presented for comparison.   For both the flaps-up and flaps-down curves, the horizontal-tail position is maintained at the pre-touchdown trim position $\delta_{h_{trim}}$.   The critical nature of landing without the use of flaps is evident, particularly if the design weight is exceeded; however, the effect of excessive weight during a flaps-down landing is small and is of less importance than a flap malfunction.   The normally detrimental effects of aerodynamic loads and weight on X-15 landing loads, which are discussed in references 3 and 4, are thus seen to be particularly severe during an emergency landing.

It is of interest to illustrate, through the use of analysis, how the aerodynamics can be used advantageously to alleviate the landing loads during emergency conditions. X-15 main-gear landing loads are presented in figure 9 as a function of weight for the severe emergency of a flap malfunction.   The horizontal-tail loads are manipulated during the landing to achieve the three curves shown.   The $\delta_{h_{trim}}$ maneuver, which was shown in figure 8, offers only limited capabilities for the emergency landing, and the normal pilot technique of pulling back on the control stick $\delta_{h_{pull}}$ is intolerable. However, the push maneuver $\delta_{h_{push}}$, discussed in references 3 and 4, in which the
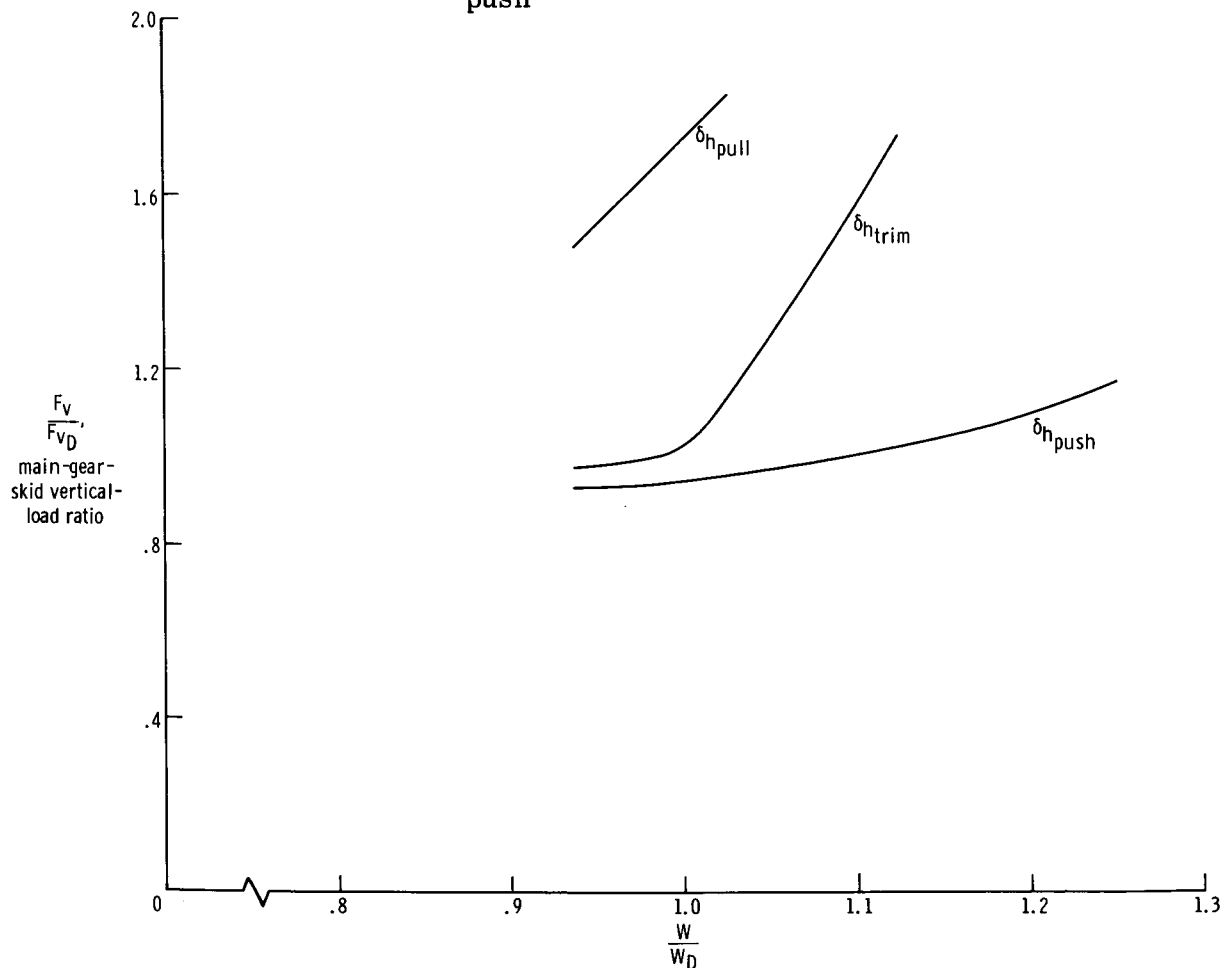

Figure 9.— Influence of horizontal-tail position on maximum main-gear load calculated by using method of

appendix A. $\dfrac{V_{v_0}}{V_{v_D}} = 0.55$; $\dfrac{a_0}{a_D} = 1.0$; $a_n = 1g$;   flaps up.

24

pilot pushes forward on the control stick at touchdown results in main-gear loads that are lower or only slightly higher than the gear design load even for severe off-design landing conditions of excessive weight and a flap malfunction. It should be pointed out that the ineffectiveness of the horizontal tail in controlling nose-gear loads, because of the location of the tail, results in only a slight increase in nose-gear load because of the push maneuver (refs. 3 and 4).

Experience with the X-15 airplane has revealed that the aerodynamic loads are extremely important to the landing dynamics because of the unusual relative location of landing gear and aerodynamic surfaces of the vehicle. Results from the analysis, such as those in figure 9, have further shown that by proper manipulation of the horizontal-tail aerodynamic loads the initially detrimental effects on landing loads can be used advantageously to expand the X-15 landing envelope to include high landing weights and no-flap emergencies.

CONCLUDING REMARKS

A theoretical analysis has been presented for the landing dynamics of a vehicle with a tricycle landing-gear system. The equations were reduced by simplifying assumptions which resulted in a modified analysis consistent with the landing dynamics of the X-15 airplane. Calculations were made with the modified analysis in order to compare the theoretical landing loads with flight- and drop-test data. Comparison of calculated results with flight-test data indicates that the modified analysis adequately simulates the landing dynamics of the X-15 airplane as well as predicts the magnitudes of the peak loads.

Parameter studies conducted for the X-15 illustrated the effects of weight, flap position, and horizontal-tail position on the main-gear loads. The results of this analysis indicate that it is possible to advantageously use the unusual relationship between the aerodynamics and the landing-gear configuration to expand the landing envelope to include higher weights and no-flap emergencies.
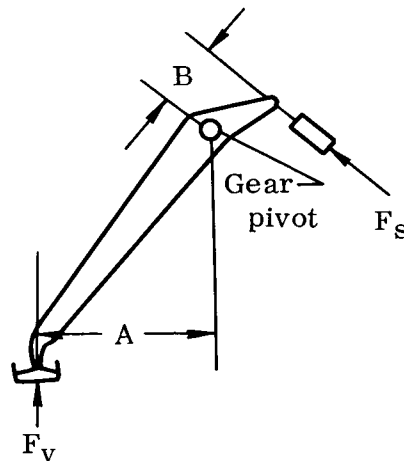
Flight Research Center,
    National Aeronautics and Space Administration,
        Edwards, Calif., May 1, 1967,
            719-01-00-04-24.

APPENDIX A

ANALYSIS OF VERTICAL LOADS ON THE X-15 LANDING GEAR

Main Gear

The X-15 main landing gear is of the articulated type, as illustrated in the sketch below. (See reference 1 for a detailed discussion.)

The ground reaction F_V is transmitted through a skid, landing-gear-leg, and bell-crank arrangement to an oleopneumatic shock strut inside the fuselage. Prior to shock-strut displacement, the vertical load is a function of the vertical skid displacement due to leg bending. The bending load can be expressed as

$$F_{\delta_i} = K\delta_{B_i} \tag{A1}$$

where K is the stiffness coefficient of the main-gear leg which relates vertical load to vertical deflection. This coefficient can be described analytically but is obtained more practically by static tests. The vertical-bending deflection δ_B is equivalent to the overall gear deflection described by equation (4) or equations (20) or (24c).

After shock-strut motion, the vertical load is expressed as in equation (3). Because of the articulated nature of the main gear, the vertical load at the ground and the shock-strut load are not equivalent; however, they can be related through the gear geometry. Equating moments about the gear pivot (see preceding sketch) results in

$$F_V = \frac{B}{A} F_S \tag{A2}$$

26

APPENDIX A

The gear vertical load is a function of the ratio $\dfrac{B}{A}$, which varies as the gear rotates about the pivot, and of the shock-strut load F_S. The load F_S is given by

$$F_S = F_{A_S} + F_{H_S} + F_{f_S} \tag{A3}$$

where the quantities are defined as for equation (3). For the X-15 airplane, the friction forces F_{f_S} are assumed to be negligible. The shock-strut airspring load F_{A_S} is determined experimentally for the X-15 but can be obtained analytically (see ref. 7). The hydraulic load F_{H_S} is related to the shock-strut velocity $\dot{\delta}_S$ by

$$F_{H_S} = C_S \dot{\delta}_S{}^2 \tag{A4}$$

where C_S is an experimentally defined hydraulic coefficient. The load does not have a direction sign as in reference 7, since the X-15 shock strut produces hydraulic load only in compression. During the expansion stroke, hydraulic pressure is relieved through orifices so that the load is the result of the airspring only. This condition is approximated by

$$F_{H_S} = 0 \quad \text{if} \quad \dot{\delta}_S \leqq 0 \tag{A5}$$

The vertical and shock-strut loads were related by equation (A2). Using the same technique

$$\dot{\delta}_S = \frac{B}{A} \dot{\delta}_{M_R} \tag{A6}$$

where $\dot{\delta}_{M_R}$ is the rate of vertical deflection of the main gear due to the rigid rotation of the gear about the pivot.

Substituting equations (A3), (A4), and (A6) into equation (A2) results in

$$F_V = F_A + C_M \dot{\delta}_{M_R}{}^2 \tag{A7}$$

where

$$F_A = \frac{B}{A} F_{A_S} \quad \text{and} \quad C_M = \left(\frac{B}{A}\right)^3 C_S$$

27

APPENDIX A

The X-15 main-gear shock strut also incorporates a pressure-relief valve which, upon opening, prevents a further increase in hydraulic pressure. Until the valve opens, the strut is velocity-sensitive, but after the orificing the strut load is the air-spring load with the pressure-limited non-velocity-sensitive hydraulic load added to it. Therefore, as long as the relief valve is open, equation (A4) becomes

$$F_{H_S} = \left(F_{H_S}\right)_{max} \tag{A8}$$

where $\left(F_{H_S}\right)_{max}$ is the maximum attainable hydraulic load.

The skid load of equation (A7) is then written

$$F_V = F_A + \left(F_H\right)_{max} \tag{A9}$$

where $\left(F_H\right)_{max} = \dfrac{B}{A}\left(F_{H_S}\right)_{max}$.

The overall vertical-deflection rate $\dot{\delta}_M$ given by equation (4) or by equations (20) or (24c) is the sum of the rates of vertical deflection or

$$\dot{\delta}_M = \dot{\delta}_B + \dot{\delta}_{M_R} \tag{A10}$$

The rate of bending deflection is now obtained by considering the main-gear leg as a single-degree-of-freedom damped spring mass. Then

$$\ddot{\delta}_B = g - \frac{K}{m_M}\delta_B - \frac{C_1}{m_M}\dot{\delta}_B + \frac{F_v}{m_M} \tag{A11}$$

where g is the gravitational acceleration, C_1 is the damping coefficient, and m_M is the mass of the main-gear leg.

Nose Gear

The X-15 nose gear is a conventional-type gear (ref. 1), utilizing dual co-rotating wheels and tires and an oleopneumatic shock strut. The vertical load F_v prior to shock-strut displacement is a function of the tire deflection δ_t or

$$F_v = F_t = f(\delta_t) \tag{A12}$$

28

APPENDIX A

where F_t is the vertical load on the tire. The relationship between F_v and δ_t is obtained experimentally for the X-15. The tire deflection is equivalent to the overall nose-gear deflection given by equation (4) or equations (20) or (24c).

After shock-strut motion, the vertical load is described by equation (3). Since gear bending has been neglected, the methods of reference 7 result in

$$F_v = F_A + C_N \dot{\delta}_s{}^2 \frac{\dot{\delta}_s}{|\dot{\delta}_s|} \tag{A13}$$

where the airspring load F_A and the hydraulic coefficient C_N are experimentally determined functions of the nose-gear shock-strut deflection δ_s.

The shock-strut deflection is related to the overall gear-deflection rate by

$$\dot{\delta}_N = \dot{\delta}_s + \dot{\delta}_t \tag{A14}$$

The rate of the tire deflection is obtained by considering the wheel and tire as a single-degree-of-freedom damped spring mass. Then

$$\ddot{\delta}_t = g + \frac{F_v - F_t}{m_N} \tag{A15}$$

where m_N is the mass of the tire and wheel.

APPENDIX B

RELATIONS FOR DROP-TEST SIMULATION

Drop tests of the X-15 landing gear were made to determine the actual gear characteristics. Each gear was tested individually rather than as a complete landing-gear system. Weight was added to the basic landing gear to simulate inertia loads due to vertical motion. Thus, equation (24a) for vertical motion becomes for each gear

$$m\ddot{z}_O = W - L - F_V \qquad\qquad (B1)$$

where L represents a simulated aerodynamic force. Equations (24c) are then replaced by

$$\dot{\delta} = \dot{z}_O \qquad\qquad (B2)$$

where initially $\dot{z}_O = V_V$.

The equations of appendix A are still applicable for the gear-drop tests. The mass m and weight W are the effective masses and weights computed for the critical landing conditions.

REFERENCES

1. McKay, James M.; and Scott, Betty J.: Landing-Gear Behavior During Touchdown and Runout for 17 Landings of the X-15 Research Airplane. NASA TM X-518, 1961.

2. McKay, James M.; and Kordes, Eldon E.: Landing Loads and Dynamics of the X-15 Airplane. NASA TM X-639, 1962.

3. Noll, Richard B.; Jarvis, Calvin R.; Pembo, Chris; Lock, Wilton P.; and Scott, Betty J.: Aerodynamic and Control-System Contributions to the X-15 Airplane Landing-Gear Loads. NASA TN D-2090, 1963.

4. McKay, James M.; and Noll, Richard B.: A Summary of the X-15 Landing Loads. NASA TN D-3263, 1966.

5. Mechtly, E. A.: The International System of Units - Physical Constants and Conversion Factors. NASA SP-7012, 1964.

6. Noll, Richard B.; and Halasey, Robert L.: Theoretical Investigation of the Slideout Dynamics of a Vehicle Equipped With a Tricycle Skid-Type Landing-Gear System. NASA TN D-1828, 1963.

7. Milwitzky, Benjamin; and Cook, Francis E.: Analysis of Landing-Gear Behavior. NACA Rep. 1154, 1953.

"The aeronautical and space activities of the United States shall be conducted so as to contribute . . . to the expansion of human knowledge of phenomena in the atmosphere and space. The Administration shall provide for the widest practicable and appropriate dissemination of information concerning its activities and the results thereof."

—NATIONAL AERONAUTICS AND SPACE ACT OF 1958

NASA SCIENTIFIC AND TECHNICAL PUBLICATIONS

TECHNICAL REPORTS: Scientific and technical information considered important, complete, and a lasting contribution to existing knowledge.

TECHNICAL NOTES: Information less broad in scope but nevertheless of importance as a contribution to existing knowledge.

TECHNICAL MEMORANDUMS: Information receiving limited distribution because of preliminary data, security classification, or other reasons.

CONTRACTOR REPORTS: Scientific and technical information generated under a NASA contract or grant and considered an important contribution to existing knowledge.

TECHNICAL TRANSLATIONS: Information published in a foreign language considered to merit NASA distribution in English.

SPECIAL PUBLICATIONS: Information derived from or of value to NASA activities. Publications include conference proceedings, monographs, data compilations, handbooks, sourcebooks, and special bibliographies.

TECHNOLOGY UTILIZATION PUBLICATIONS: Information on technology used by NASA that may be of particular interest in commercial and other non-aerospace applications. Publications include Tech Briefs, Technology Utilization Reports and Notes, and Technology Surveys.

Details on the availability of these publications may be obtained from:

SCIENTIFIC AND TECHNICAL INFORMATION DIVISION
NATIONAL AERONAUTICS AND SPACE ADMINISTRATION
Washington, D.C. 20546